

AD-A059 881

NAVAL RESEARCH LAB WASHINGTON D C
FULLY MULTIDIMENSIONAL FLUX-CORRECTED TRANSPORT. (U)
MAY 78 S T ZALESAK

F/G 20/4

UNCLASSIFIED

NRL-MR-3716

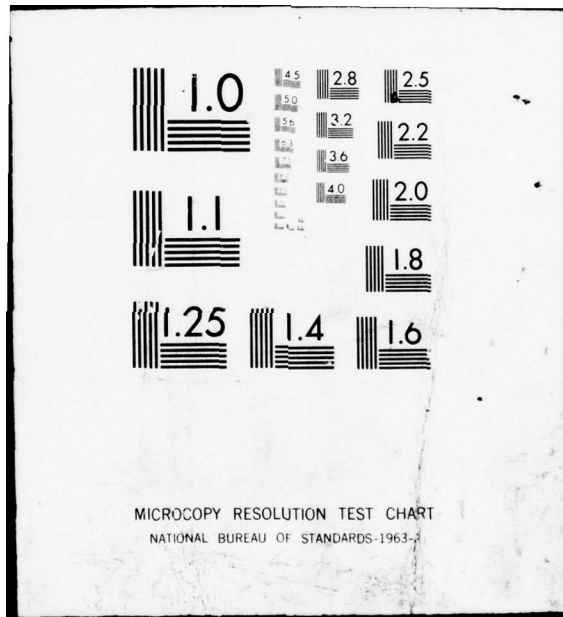
SBIE-AD-E000 206

NL

1 OF 1
AD
A059881



END
DATE
FILMED
12-78
DDC



ADA059881

AD-E 000206

NRL Memorandum Report 3716

(12)
NW

Fully Multidimensional Flux-Corrected Transport

STEVEN T. ZALESAK

Plasma Dynamics Branch
Plasma Physics Division

LEVEL II

May 1978

DDC FILE COPY

This research was supported by the Defense Nuclear Agency under Subtask S99AXHC041,
Work Unit 12 and Work Unit Title "Ionization Structure Research."



D D C
REFINED
OCT 17 1978
B

NAVAL RESEARCH LABORATORY
Washington, D.C.

Approved for public release: distribution unlimited.

78 08 16 09 0

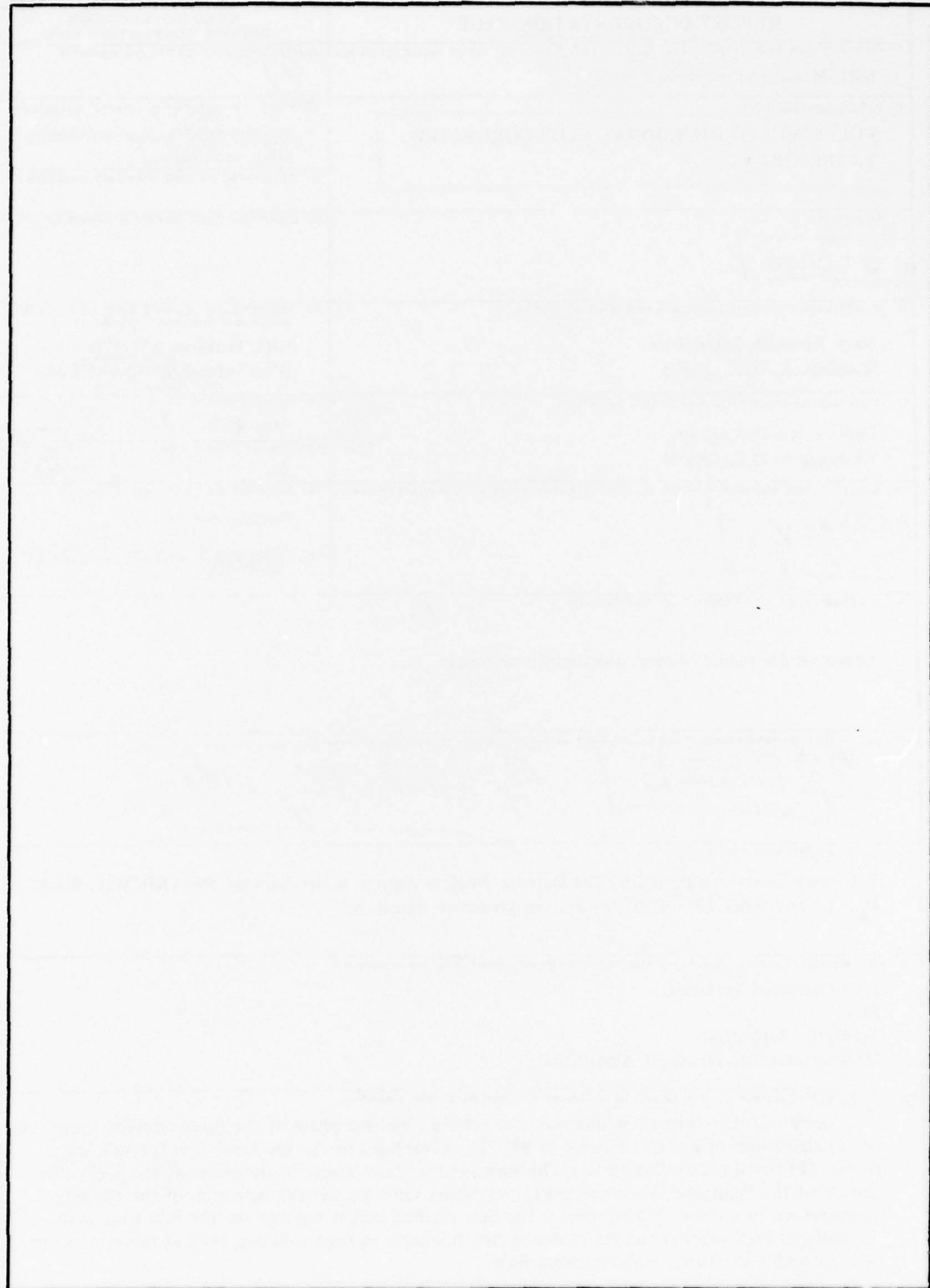
SECURITY CLASSIFICATION OF THIS PAGE (When Data Entered)

REPORT DOCUMENTATION PAGE			READ INSTRUCTIONS BEFORE COMPLETING FORM
1. REPORT NUMBER NRL Memorandum Report 3716	2. GOVT ACCESSION NO.	3. RECIPIENT'S CATALOG NUMBER ⑨	
4. TITLE (and Subtitle) FULLY MULTIDIMENSIONAL FLUX-CORRECTED TRANSPORT •		5. TYPE OF REPORT & PERIOD COVERED Interim report on a continuing NRL problem.	
6. AUTHOR(s) Steven T. Zalesak		7. CONTRACT OR GRANT NUMBER(s)	
8. PERFORMING ORGANIZATION NAME AND ADDRESS Navy Research Laboratory Washington, D.C. 20375		9. PROGRAM ELEMENT, PROJECT, TASK AREA & WORK UNIT NUMBERS NRL Problem H02-27B DNA Subtask S99QAXHC041	
10. CONTROLLING OFFICE NAME AND ADDRESS Defense Nuclear Agency Washington, D.C. 20305		11. REPORT DATE May 1978	
12. NUMBER OF PAGES 48		13. SECURITY CLASS. (of this report) Unclassified	
14. MONITORING AGENCY NAME & ADDRESS (if different from Controlling Office) ⑫ DIA		15a. DECLASSIFICATION/DOWNGRADING SCHEDULE	
16. DISTRIBUTION STATEMENT (of this Report) Approved for public release; distribution unlimited.			
17. DISTRIBUTION STATEMENT (of the abstract entered in Block 20, if different from Report) ⑯ SRBIE ⑯ AD-E000/206			
18. SUPPLEMENTARY NOTES This research was supported by the Defense Nuclear Agency under Subtask S99AXHC041, Work Unit 12 and Work Unit Title "Ionization Structure Research."			
19. KEY WORDS (Continue on reverse side if necessary and identify by block number) Flux-Corrected Transport FCT Transport Algorithms Multidimensional Transport Algorithms			
20. ABSTRACT (Continue on reverse side if necessary and identify by block number) An alternative formula is proposed for the flux limiting phase of the flux-corrected transport (FCT) algorithms of Boris and Book [1-3]. The advantages of the proposed new formula are three: (1) trivial generalization to multidimensions without resort to time-step splitting; (2) elimination of the "clipping" phenomenon for vanishing velocity; and (3) reduction of the clipping phenomenon in a finite velocity field. The new method makes possible for the first time multidimensional FCT calculations for problems not amenable to time splitting, such as those involving incompressible or nearly incompressible flow.			

251 950

RP

SECURITY CLASSIFICATION OF THIS PAGE (When Data Entered)



SECURITY CLASSIFICATION OF THIS PAGE(When Data Entered)

CONTENTS

I. INTRODUCTION: FCT DEFINED	1
II. MULTIDIMENSIONAL FLUX-CORRECTED TRANSPORT	2
III. FLUX LIMITING IN ONE SPATIAL DIMENSION – THE ORIGINAL ALGORITHM	4
IV. FLUX LIMITING IN ONE SPATIAL DIMENSION – AN ALTERNATIVE ALGORITHM	6
V. COMPUTATIONAL EXAMPLES – ONE DIMENSION	8
VI. FLUX LIMITING IN MULTIDIMENSIONS	11
VII. COMPUTATIONAL EXAMPLES – TWO DIMENSIONS	12
VIII. THE STRIATIONS CODE – A TWO DIMENSIONAL INCOMPRESSIBLE FLUID CODE USING FULLY MULTIDIMENSIONAL FCT	14
CONCLUSIONS	15
ACKNOWLEDGMENTS	17
REFERENCES	17
APPENDIX – Brief Description of Leapfrog-Trapezoidal Transport Algorithms	18

ACCESSION for	
NTIS	White Section <input checked="" type="checkbox"/>
DDC	Buff Section <input type="checkbox"/>
UNANNOUNCED <input type="checkbox"/>	
JUSTIFICATION	
BY	
DISTRIBUTION/AVAILABILITY CODES	
Dist. AVAIL. and/or SPECIAL	
A	

FULLY MULTIDIMENSIONAL FLUX-CORRECTED TRANSPORT

I. INTRODUCTION: FCT DEFINED

Consider the following system of equations

$$w_t + f_x = 0 \quad (1)$$

where w and f are vector functions of independent variables x and t . A simple example of such a system of equations would be the one dimensional equations of ideal, inviscid fluid flow:

$$w = \begin{pmatrix} \rho \\ \rho v \\ \rho E \end{pmatrix}; \quad f = \begin{pmatrix} \rho v \\ \rho v^2 + P \\ \rho v E + P v \end{pmatrix}$$

where ρ , v , P and E are the fluid density, velocity, hydrostatic pressure and specific total energy respectively.

We shall say that a finite difference approximation to Eq. (1) is in conservation (or "flux") form when it can be written in the form

$$w_i^{n+1} = w_i^n - \Delta x_i^{-1} [F_{i+(1/2)} - F_{i-(1/2)}] \quad (2)$$

Here w and f are defined at the spatial grid points x_i and temporal grid points t^n , and $\Delta x_i \equiv \frac{1}{2} (x_{i+1} - x_{i-1})$. The $F_{i+(1/2)}$ are called transportive fluxes, and are functions of f at one or more of the time levels t^n . The functional dependence of F on f defines the integration scheme (leapfrog, Lax-Wendroff, Crank Nicholson, donor cell, etc.).

It is well known that higher order (order 2 and above) schemes for numerically integrating Eq. (1) suffer from dispersive "ripples" in w , particularly near steep gradients in w . Lower order schemes, such as donor cell, Lax-Friedrichs, or high order schemes with a zeroth order diffusion added, produce no ripples but suffer from excessive numerical diffusion. Flux-corrected transport (FCT) is a technique developed by Boris and Book [1-3] which embodies the best of both of the above worlds. In its simplest terms, FCT constructs the net transportive flux point by point (*non* linearly) as a weighted average of a flux computed by a low order scheme and a flux computed by a high order scheme. The weighting is done in a manner which insures that the high order flux is used to the greatest extent possible without introducing rip-

*Manuscript submitted May 17, 1978.

ples (overshoots and undershoots). This weighting procedure is referred to as "flux-correction" or "flux-limiting" for reasons which shall become clear later. The result is a family of transport algorithms capable of resolving moving contact discontinuities over 3-4 grid points, and shock fronts over 2 grid points, *without* undershoot or overshoot [1-3]. Formally, the procedure is as follows:

- 1) Compute $F_{i+(1/2)}^L$, the transportive flux given by some low order scheme guaranteed to give monotonic (ripple-free) results for the problem at hand
- 2) Compute $F_{i+(1/2)}^H$, the transportive flux given by some high order scheme
- 3) Define the "antidiffusive flux":

$$A_{i+(1/2)} \equiv F_{i+(1/2)}^H - F_{i+(1/2)}^L$$

- 4) Compute the updated low order ("transported and diffused") solution:

$$w_i^{ld} = w_i^n - \Delta x_i^{-1} \left[F_{i+(1/2)}^L - F_{i-(1/2)}^L \right]$$

- 5) Limit the $A_{i+(1/2)}$ in a manner such that w^{n+1} as computed in step 6 below is free of overshoots and undershoots:

$$A_{i+(1/2)}^C = C_{i+(1/2)} A_{i+(1/2)}, \quad 0 \leq C_{i+(1/2)} \leq 1$$

- 6) Apply the limited antidiffusive fluxes:

$$w_i^{n+1} = w_i^{ld} - \Delta x_i^{-1} \left[A_{i+(1/2)}^C - A_{i-(1/2)}^C \right]$$

The critical step in the above is, of course, step 5 which will be discussed shortly. In the absence of the flux limiting step ($A_{i+(1/2)}^C = A_{i+(1/2)}$), w_i^{n+1} would simply be the time-advanced, high order solution.

We note that this definition of FCT is considerably more general than has been given previously.

II. MULTIDIMENSIONAL FLUX-CORRECTED TRANSPORT

Before proceeding to a discussion of flux limiting, let us see how the procedure given above might be implemented in multidimensions. An obvious choice would be to use a Strang-type time-splitting procedure [4] when it can be shown that the equations allow such a

technique to be used without serious error. Indeed, such a procedure may even be preferable from programming and time-step considerations. However, there are many problems for which time-splitting produces unacceptable numerical results, among which are those involving incompressible or nearly incompressible flow fields. This technique is straightforward and shall not be discussed here. Instead we consider as an example the fully two-dimensional set of equations

$$w_t + f_x + g_y = 0 \quad (3)$$

where w , f , and g are vector functions of x , y , and t . In finite difference flux form we have

$$w_{i,j}^{n+1} = w_{i,j}^n - \Delta V_{i,j}^{-1} \left[F_{i+(1/2),j} - F_{i-(1/2),j} + G_{i,j+(1/2)} - G_{i,j-(1/2)} \right] \quad (4)$$

where now w , f and g are defined on spatial grid points x_i , y_j at time levels t^n , and $\Delta V_{i,j}$ is a two dimensional area element centered on grid point (i, j) . Now there are two sets of transportive fluxes F and G , and the FCT algorithm proceeds as before:

- 1) Compute $F_{i+(1/2),j}^L$ and $G_{i,j+(1/2)}^L$ by a low order monotonic scheme
- 2) Compute $F_{i+(1/2),j}^H$ and $G_{i,j+(1/2)}^H$ by a high order scheme
- 3) Define the antidiiffusive fluxes:

$$A_{i+(1/2),j} \equiv F_{i+(1/2),j}^H - F_{i+(1/2),j}^L$$

$$A_{i,j+(1/2)} \equiv G_{i,j+(1/2)}^H - G_{i,j+(1/2)}^L$$

- 4) Compute the low order time advanced solution:

$$w_{i,j}^{td} = w_{i,j}^n - \Delta V_{i,j}^{-1} \left[F_{i+(1/2),j}^L - F_{i-(1/2),j}^L + G_{i,j+(1/2)}^L - G_{i,j-(1/2)}^L \right]$$

- 5) Limit the antidiiffusive fluxes

$$A_{i+(1/2),j}^C = A_{i+(1/2),j} C_{i+(1/2),j} \quad 0 \leq C_{i+(1/2),j} \leq 1$$

$$A_{i,j+(1/2)}^C = A_{i,j+(1/2),j} C_{i,j+(1/2)} \quad 0 \leq C_{i,j+(1/2)} \leq 1$$

- 6) Apply the limited antidiiffusive fluxes:

$$w_{i,j}^{n+1} = w_{i,j}^{td} - \Delta V_{i,j}^{-1} \left[A_{i+(1/2),j}^C - A_{i-(1/2),j}^C + A_{i,j+(1/2)}^C - A_{i,j-(1/2)}^C \right]$$

As can be easily seen, implementation of FCT in multidimensions is straightforward with the exception of Step 5, an algorithm for which is the subject of this paper. First, however, let

us see how flux limiting is presently implemented in one spatial dimension.

III. FLUX LIMITING IN ONE SPATIAL DIMENSION – THE ORIGINAL ALGORITHM

The original algorithm for flux-limiting in one dimension was given by Boris and Book [1]. In our notation it is:

$$A_{i+(1/2)}^C = S_{i+(1/2)} \max \left\{ 0, \min \left[|A_{i+(1/2)}|, S_{i+(1/2)} \left(w_{i+2}^{id} - w_{i+1}^{id} \right) \Delta x_{i+1}, S_{i+(1/2)} \left(w_i^{id} - w_{i-1}^{id} \right) \Delta x_{i-1} \right] \right\} \quad (5)$$

where

$$S_{i+(1/2)} = \begin{cases} +1 & \text{if } A_{i+(1/2)} \geq 0 \\ -1 & \text{if } A_{i+(1/2)} < 0 \end{cases}$$

The intent of this formula is that antidiiffusive fluxes should neither create new extrema, nor accentuate already existing extrema, in the transported and diffused solution w^{id} . That the above formula does, in fact, perform precisely this task can be verified by the reader with relative ease. We shall examine here some of the less obvious properties of this very powerful, yet simple, formula. In the process we shall gain insight into which of these properties we shall wish to carry over into a multidimensional flux limiter. We first observe that certain quantities do *not* appear in the above formula: 1) $w_{i+1}^{id} - w_i^{id}$, the first difference of w^{id} at the point where the antidiiffusive flux $A_{i+(1/2)}$ is evaluated; and 2) antidiiffusive fluxes other than $A_{i+(1/2)}$. This last property is the most notable since there are conceivably two fluxes directed into or out of a cell. A formula guaranteeing that the two fluxes *acting in concert* shall not create ripples would apparently require a knowledge of *both*. We shall return to this point momentarily.

In Figure 1 we show the eight possible configurations of w^{id} in the neighborhood of a positive $A_{i+(1/2)}$ (directed to the right in our diagrams). Configurations 1-4 show the "normal" situation, with $A_{i+(1/2)}$ having the same sign as $w_{i+1}^{id} - w_i^{id}$ (as might be expected of an "antidiiffusive flux"). We note that if either $w_{i+2}^{id} - w_{i+1}^{id}$ or $w_i^{id} - w_{i-1}^{id}$ has a sign opposed to that of $A_{i+(1/2)}$, as in configurations 2-4, the antidiiffusive flux $A_{i+(1/2)}$ is *completely canceled*. This,

however, is in total agreement with the stated intent of Eq. (5) since otherwise configuration 2 would allow accentuation of an existing maximum, configuration 3 accentuation of an existing minimum, and configuration 4 accentuation of both. In the remaining configuration 1, the flux limiter (5) will reduce the magnitude of $A_{i+(1/2)}$ sufficiently to guarantee that neither a maximum at grid point $i + 1$ nor a minimum at grid point i will be formed, again in precise agreement with its stated intent.

Configurations 5-8 are identical to configurations 1-4, respectively, except that sign of $w_{i+1}^{id} - w_i^{id}$ has been reversed (The "antidiffusive fluxes" are now directed *down* the gradient in w^{id}). Since the sign of $w_{i+1}^{id} - w_i^{id}$ does not enter into the flux correction formula (5), the results of the formula are identical to those for the previous four cases: the antidiffusive fluxes are canceled for configurations 6-8 and limited in configuration 5 to the extent necessary to prevent a new maximum at grid point $i + 1$ and a new minimum at grid point i . Examination of configurations 6-8 reveals that $A_{i+(1/2)}$ actually presented no hazard insofar as extrema creation or enhancement (at least in moderation). Certainly there was no cause for completely canceling the flux. Even in configuration 5 the flux may have been limited to a greater extent than necessary. At first it would seem that configurations 5-8 represent errors introduced by the simplicity of the flux limiting formula (5). However, extensive tests by this author indicate that in the relatively rare instances in which configurations 5-8 occur in practice, the "errors" introduced by Eq. (5) represent, in fact, the correct action to take in terms of producing accurate profiles in w^{n+1} . More importantly, they represent the mechanism by which Eq. (5) can guarantee that ripples are not formed under any circumstances, as we shall see presently.

Consider two antidiffusive fluxes, acting in concert, attempting to produce or accentuate an extremum. We therefore have $A_{i+(1/2)}$ and $A_{i-(1/2)}$ either both directed toward, or both directed away from grid point i . We see from Figure 1 that, in general, an antidiffusive flux directed opposite to the gradient in w^{id} will be completely canceled. Therefore the only cases of fluxes acting in concert that we need be concerned with are those where two adjacent fluxes are both parallel to the local gradients in w^{id} . These are precisely the cases of already existing

extrema, in which case *both* fluxes will be canceled (as in configurations 2-4). This is the reason that Eq. (5) needs no information on any antidiiffusive flux other than $A_{i+(1/2)}$.

In Figure 2 we see that the above-mentioned assumptions regarding antidiiffusive fluxes acting in concert break down completely in multidimensions. It is possible in more than one dimension for more than one antidiiffusive flux to be directed into or out of a cell, all of these fluxes being directed parallel to the local gradient in w^{id} , without that cell being an already existing extremum. Therefore the problem of dealing with multiple antidiiffusive fluxes acting in concert cannot be avoided by simply canceling all fluxes antiparallel to the local gradient in w^{id} . It is clear then that any formula which purports to perform flux limiting in more than one dimension without resort to time splitting *must* contain information about antidiiffusive fluxes other than the one being limited.

IV. FLUX LIMITING IN ONE SPATIAL DIMENSION – AN ALTERNATIVE ALGORITHM

We describe here in one spatial dimension an alternative flux limiting algorithm which generalizes easily to multidimensions and which, even in one dimension, exhibits a superiority to the limiter described in the previous section (Eq. (5)) with regard to peaked profiles.

Referring to Figure 3, we seek to limit the antidiiffusive flux $A_{i+(1/2)}$ such that

$$A_{i+(1/2)}^C = C_{i+(1/2)} A_{i+(1/2)}, \quad 0 \leq C_{i+(1/2)} \leq 1 \quad (6)$$

and such that $A_{i+(1/2)}^C$ acting in concert with $A_{i-(1/2)}^C$ will not allow

$$w_i^{n+1} = w_i^{id} - \Delta x_i^{-1} [A_{i+(1/2)}^C - A_{i-(1/2)}^C]$$

to exceed some maximum value w_i^{\max} nor fall below some minimum value w_i^{\min} . We leave the determination of w_i^{\max} and w_i^{\min} until later.

We define three quantities:

$P_i^+ =$ the sum of all antidiiffusive fluxes *into* grid point i

$$= \max (0, A_{i-(1/2)}) - \min (0, A_{i+(1/2)}) \quad (7)$$

$$Q_i^+ = (w_i^{\max} - w_i^{id}) \Delta x_i \quad (8)$$

$$R_i^+ = \begin{cases} \min(1, Q_i^+/P_i^+) & \text{if } P_i^+ > 0 \\ 0 & \text{if } P_i^+ = 0 \end{cases} \quad (9)$$

Assuming that $w_i^{\max} \geq w_i^{id}$ (it *must* be), all three of the above quantities are positive and R_i^+ represents the least upper bound on the fraction which must multiply all antidiffusive fluxes *into* grid point i to guarantee no overshoot at grid point i .

Similarly we define three corresponding quantities:

P_i^- = the sum of all antidiffusive fluxes *away from* grid point i

$$= \max(0, A_{i+(1/2)}) - \min(0, A_{i-(1/2)}) \quad (10)$$

$$Q_i^- = (w_i^{id} - w_i^{\min}) \Delta x_i \quad (11)$$

$$R_i^- = \begin{cases} \min(1, Q_i^-/P_i^-) & \text{if } P_i^- > 0 \\ 0 & \text{if } P_i^- = 0 \end{cases} \quad (12)$$

Again assuming that $w_i^{\min} \leq w_i^{id}$, we find that R_i^- represents the least upper bound on the fraction which must multiply all antidiffusive fluxes *away from* grid point i to guarantee no undershoot at grid point i .

Finally we observe that all antidiffusive fluxes are directed away from one grid point and into an adjacent one. Limiting will therefore take place with respect to undershoots for the former and with respect to overshoots for the latter. A guarantee that neither event comes to pass demands our taking a minimum:

$$C_{i+(1/2)} = \begin{cases} \min(R_{i+1}^+, R_i^-) & \text{if } A_{i+(1/2)} \geq 0 \\ \min(R_i^+, R_{i+1}^-) & \text{if } A_{i+(1/2)} < 0 \end{cases} \quad (13)$$

Furthermore, we shall call upon our previously described experience with the original flux limiter and set

$$A_{i+(1/2)} = 0 \text{ if } A_{i+(1/2)} (w_{i+1}^{id} - w_i^{id}) < 0 \quad (14)$$

and either $A_{i+(1/2)} (w_{i+2}^{id} - w_{i+1}^{id}) < 0$

or $A_{i+(1/2)} (w_i^{id} - w_{i-1}^{id}) < 0$

In practice the effect of Eq. (14) is minimal and is primarily cosmetic in nature. This is because cases of antidiffusive fluxes directed down gradients in w^{id} are rare, and even when they occur usually involve flux magnitudes that are small compared to adjacent fluxes. If Eq. (14) is used, it should be applied *before* Eq. (6) through (13).

We come now to a determination of the quantities w_i^{\max} and w_i^{\min} in Eqs. (8) and (11).

A safe choice is

$$w_i^{\max} = \max (w_{i-1}^{td}, w_i^{td}, w_{i+1}^{td}) \quad (15)$$

$$w_i^{\min} = \min (w_{i-1}^{td}, w_i^{td}, w_{i+1}^{td}) \quad (16)$$

This choice will produce results identical with those of Eq. (5) in one dimension, including the occurrence of the "clipping" phenomenon to be mentioned shortly.

A better choice is:

$$w_i^a = \max (w_i^n, w_i^{td})$$

$$w_i^{\max} = \max (w_{i-1}^a, w_i^a, w_{i+1}^a) \quad (17)$$

$$w_i^b = \min (w_i^n, w_i^{td})$$

$$w_i^{\min} = \min (w_{i-1}^b, w_i^b, w_{i+1}^b) \quad (18)$$

This choice allows us to look back to the previous time step for upper and lower bounds on w_i^{n+1} .

It is clear that these two methods of determining w_i^{\max} and w_i^{\min} represent only a small subset of possible methods. The alternative flux limiter described in equations (6) through (14) admits of any physically motivated upper and lower bound on w_i^{n+1} supplied by the user, introducing a flexibility unavailable with the original flux limiter (5). However, with the exception of one example in the next section (which shows graphically the potential power of this flexibility), we shall henceforth use Eq. (17) and (18) to evaluate w^{\min} and w^{\max} in one dimension.

V. COMPUTATIONAL EXAMPLES – ONE DIMENSION

We consider one dimensional passive convection in a constant velocity field. We have Eq. (1) with $w = \rho$ and $f = \rho v$ with $v = \text{constant}$. We choose our transport algorithm to be that given in [3] for LPE Shasta. On the standard square wave tests we find that our results for the original flux limiter (5) and for the alternative flux limiter (6) through (14) are identical to within round-off (the same is true for traveling shock waves in the coupled one dimensional equations of ideal inviscid fluid flow). To find differences between the limiters in one dimension we must look to passive convection of peaked profiles. We choose the problem given by Forester [5], a gaussian of half-width $2\Delta x$. In Figure 4 we show the results after 600 iterations

for the trivial case $v = 0$. On the left we see the similar "clipping" phenomenon with the original flux limiter, caused by a zeroth order diffusion term in the low order portion of the LPE Shasta algorithm. This diffusion term causes the peak in w^{ld} to be smaller than the peak in w' , leaving the original flux limiter (5) with no way of resurrecting the original peak. This process occurs repeatedly, eventually leaving the characteristic three point top. The alternative flux limiter, shown on the right, "remembers" the old value of the peak and is able to resurrect it each time step.

In Figure 5 we show the same problem after 600 iterations but this time for $\epsilon \equiv v \Delta t / \Delta x = 0.1$. We see that clipping occurs with both flux limiters, but to a lesser extent with the alternative flux limiter (6) through (14).

At this point we removed the flux limiter entirely and again ran the problem 600 iterations with $\epsilon = 0.1$. The results convinced us that the amplitude and phase properties of the high order portion of LPE Shasta were incapable of resolving the high wave numbers of which the gaussian is composed. Consequently it was decided to switch to a higher order algorithm, a leapfrog-trapezoidal transport algorithm which uses eighth order spatial differences. The algorithm is, then, second order accurate in time and eighth order in space, with an amplification factor that is effectively unity across the entire Fourier spectrum, and phase properties considerably better than those of fourth order algorithms. The leapfrog portion of this algorithm is identical to the eighth order Kreiss-Oliger scheme [6]. A fourth order version of this same algorithm was used later in the two-dimensional solid body rotation tests. We ran the gaussian test problem again 600 iterations with $\epsilon = 0.1$ with *no* flux limiter and were convinced that the algorithm did indeed have the resolving power necessary to do the problem. A low order scheme, donor cell plus a zeroth order diffusion term with coefficient $\frac{1}{8}$, was added to complete the FCT algorithm, which we dub 2-8 leapfrog-trapezoidal. A more detailed description of this algorithm is found in the appendix.

Figure 6 shows the results of 2-8 leapfrog trapezoidal run 600 iterations with $\epsilon = 0.1$ with both the original and alternative flux limiters. The results are better than those in Figure 5,

and again the alternative flux limiter proves superior, but nonetheless disappointing. The clipping would appear to be due entirely to the flux limiters, not to the phase or amplitude properties of the high order scheme.

A careful examination of exactly what happens to a one point peak in a finite difference code reveals the real source of the above problem. Consider a profile with a local peak at grid point i in passive convection at constant velocity > 0 . At each succeeding time step the function value at grid point i will decrease and that at $i + 1$ will increase (Figure 7). Eventually they will both reach some intermediate value, and the actual original peak value will not appear anywhere on the grid, since its position now lies midway between two grid points. At this point even the new flux limiter (6) through (14), (17) and (18), has lost the information it needs to allow the peak to be resurrected in succeeding time steps, and will "clip" the new peak at grid point $i + 1$ as it tries to form, based on the assumption that it is, in fact, an overshoot. The effect is magnified, since the clipping itself introduces phase errors in succeeding iterations, the net result being the profiles depicted in Figure 6.

It is clear, then, that if we are to successfully treat a one-point extremum within the context of FCT we must use information other than just the grid point values themselves. In what follows we shall utilize the flexibility of the alternative flux limiter to use as w_i^{\max} and w_i^{\min} any values that we choose. In Figure 8 we show a possible way of extracting information about extrema which do not lie exactly on a grid point at the time. Basically we define $w_{i+(1/2)}^{\text{peak}}$ to be the w value at the intersection of the line segments formed by connecting the point (x_{i-1}, w_{i-1}^{ld}) with (x_i, w_i^{ld}) and the point (x_{i+1}, w_{i+1}^{ld}) with (x_{i+2}, w_{i+2}^{ld}) . If the x coordinate of this intersection lies between x_i and x_{i+1} , then we consider this $w_{i+(1/2)}^{\text{peak}}$ to be an allowable w^{\max} or w^{\min} for either w_i^{n+1} or w_{i+1}^{n+1} . We now have

$$w_i^a = \max (w_i^n, w_i^{ld}) \quad w_i^{\max} = \max (w_{i-1}^a, w_i^a, w_{i+1}^a, w_{i+(1/2)}^{\text{peak}}, w_{i-(1/2)}^{\text{peak}}) \quad (19)$$

$$w_i^b = \min (w_i^n, w_i^{ld}) \quad w_i^{\min} = \min (w_{i-1}^b, w_i^b, w_{i+1}^b, w_{i+(1/2)}^{\text{peak}}, w_{i-(1/2)}^{\text{peak}}) \quad (20)$$

Equations (19) and (20) together with equations (6) through (14) now determine the

alternative flux limiter (for this section only).

In Figure 9 we show the results of using Equations (19) and (20) to determine w_i^{\max} and w_i^{\min} on the gaussian test problem run 600 iterations with $\epsilon = 0.1$. Clearly the problem has been solved — we recover the gaussian profile with no dispersive ripples and minimal loss in amplitude. We have not performed this test merely to show the power of the extrapolation technique just described to determine w_i^{\max} and w_i^{\min} . *Rather this calculation serves to show the power of using information other than that available on the one dimensional grid.* In multidimensional flux limiting, this information comes from the other coordinate directions, as we shall see.

VI. FLUX LIMITING IN MULTIDIMENSIONS

The alternative flux limiting algorithm presented in section IV generalizes trivially to any number of dimensions. For the sake of completeness we present here the algorithm for two spatial dimensions.

Referring to Figure 10, we seek to limit the antidiiffusive fluxes $A_{i+(1/2), j}$ and $A_{i, j+(1/2)}$ such that

$$\begin{aligned} A_{i+(1/2), j}^C &= C_{i+(1/2), j} A_{i+(1/2), j} & 0 \leq C_{i+(1/2), j} \leq 1 \\ A_{i, j+(1/2)}^C &= C_{i, j+(1/2)} A_{i, j+(1/2)} & 0 \leq C_{i, j+(1/2)} \leq 1 \end{aligned} \quad (6')$$

and such that $A_{i+(1/2), j}^C$, $A_{i-(1/2), j}^C$, $A_{i, j+(1/2)}^C$, and $A_{i, j-(1/2)}^C$ acting in concert shall not cause

$$w_{i, j}^{n+1} = w_{i, j}^{id} - \Delta V_{i, j}^{-1} \left[A_{i+(1/2), j}^C - A_{i-(1/2), j}^C + A_{i, j+(1/2)}^C - A_{i, j-(1/2)}^C \right]$$

to exceed some maximum value $w_{i, j}^{\max}$ nor fall below some minimum value $w_{i, j}^{\min}$.

Again we compute six quantities completely analogous to those computed in Eq. (7) through (12):

$$P_{i, j}^+ = \text{the sum of all antidiiffusive fluxes into grid point } (i, j) \quad (7)$$

$$\begin{aligned} &= \max (0, A_{i-(1/2), j}) - \min (0, A_{i+(1/2), j}) \\ &+ \max (0, A_{i, j-(1/2)}) - \min (0, A_{i, j+(1/2)}) \end{aligned}$$

$$Q_{i, j}^+ = (w_{i, j}^{\max} - w_{i, j}^{id}) \Delta V_{i, j} \quad (8')$$

$$R_{i, j}^+ = \begin{cases} \min(1, Q_{i, j}^+/P_{i, j}^+) & \text{if } P_{i, j}^+ > 0 \\ 0 & \text{if } P_{i, j}^+ = 0 \end{cases} \quad (9')$$

$P_{i,j}^-$ = the sum of all antidiffusive fluxes *away from* grid point (i, j)

$$= \max(0, A_{i+(1/2), j}) - \min(0, A_{i-(1/2), j}) \quad (10')$$

$$+ \max(0, A_{i, j+(1/2)}) - \min(0, A_{i, j-(1/2)})$$

$$Q_{i,j}^- = (w_{i,j}^{id} - w_{i,j}^{\min}) \Delta V_{i,j} \quad (11')$$

$$R_{i,j}^- = \begin{cases} \min(1, Q_{i,j}^- / P_{i,j}^-) & \text{if } P_{i,j}^- > 0 \\ 0 & \text{if } P_{i,j}^- = 0 \end{cases} \quad (12')$$

Equation (13) becomes

$$C_{i+(1/2), j} = \begin{cases} \min(R_{i+1,j}^+, R_{i,j}^-) & \text{if } A_{i+(1/2), j} \geq 0 \\ \min(R_{i,j}^+, R_{i+1,j}^-) & \text{if } A_{i+(1/2), j} < 0 \end{cases}$$

$$C_{i, j+(1/2)} = \begin{cases} \min(R_{i,j+1}^+, R_{i,j}^-) & \text{if } A_{i,j+(1/2)} \geq 0 \\ \min(R_{i,j}^+, R_{i,j+1}^-) & \text{if } A_{i,j+(1/2)} < 0 \end{cases} \quad (13')$$

while Eq. (14) becomes

$$A_{i+(1/2), j} = 0 \text{ if } A_{i+(1/2), j} (w_{i+1,j}^{id} - w_{i,j}^{id}) < 0$$

and either $A_{i+(1/2), j} (w_{i+2,j}^{id} - w_{i+1,j}^{id}) < 0$
or $A_{i+(1/2), j} (w_{i,j}^{id} - w_{i-1,j}^{id}) < 0$

$$A_{i, j+(1/2)} = 0 \text{ if } A_{i, j+(1/2)} (w_{i,j+1}^{id} - w_{i,j}^{id}) < 0$$

and either $A_{i, j+(1/2)} (w_{i,j+2}^{id} - w_{i,j+1}^{id}) < 0$
or $A_{i, j+(1/2)} (w_{i,j}^{id} - w_{i,j-1}^{id}) < 0 \quad (14')$

and Eq. (17) and (18) become

$$w_{i,j}^a = \max(w_{i,j}^n, w_{i,j}^{id})$$

$$w_{i,j}^{\max} = \max(w_{i-1,j}^a, w_{i,j}^a, w_{i+1,j}^a, w_{i,j-1}^a, w_{i,j+1}^a) \quad (17')$$

$$w_{i,j}^b = \min(w_{i,j}^n, w_{i,j}^{id})$$

$$w_{i,j}^{\min} = \min(w_{i-1,j}^b, w_{i,j}^b, w_{i+1,j}^b, w_{i,j-1}^b, w_{i,j+1}^b) \quad (18')$$

Again, the effect of Eq. (14') is minimal, but if it is used it should be applied *before* Eq. (6') through (13'). Note that our search for $w_{i,j}^{\max}$ and $w_{i,j}^{\min}$ now extends over both coordinate directions. Where finite gradients exist in both directions, this procedure will allow us to stop the clipping phenomenon in regions where a peak exists with respect to one coordinate direction but not in the other, as we shall see in the next section.

VII. COMPUTATIONAL EXAMPLES – TWO DIMENSIONS

We choose as our two dimensional test problem that of solid body rotation. That is, we have Eq. (3) with $f = w v_x$, $g = w v_y$, $v_x = -\Omega(y - y_o)$, and $v_y = \Omega(x - x_o)$. Here Ω is the

(constant) angular velocity in radians/sec and (x_0, y_0) is the axis of rotation. The configuration is shown in Figure 11. The computational grid is 100×100 cells, $\Delta x = \Delta y$, with counterclockwise rotation taking place about grid point $(50, 50)$. Centered at grid point $(50, 75)$ is a cylinder of radius 15 grid points, through which a slot has been cut of width 5 grid points. The time step and rotational speed are chosen such that 628 time steps will effect one complete revolution of the cylinder about the central point. A perspective view of the initial conditions is shown in Figure 12.

Our high order scheme for the following tests is a fully two dimensional, fourth order in space, second order in time leapfrog-trapezoidal scheme, the leapfrog step of which is a two dimensional fourth order Kreiss-Oliger scheme [6]. The low order scheme is simply two dimensional donor cell plus a two dimensional zeroth order diffusion term with diffusion coefficient $\frac{1}{8}$. A more detailed description of this algorithm is found in the appendix.

We wish to emphasize that the *only* difference between calculations in the following comparisons is in the flux limiting stage itself. The high order fluxes, low order fluxes, and hence the (unlimited) antidiiffusive fluxes are all computed in the full two dimensions without using time-splitting. In each case we are comparing the fully two dimensional flux limiter given by Eq. (6') through (14'), (17') and (18') with a *time split* application of Eq. (5). Time splitting is the only way that Eq. (5) may be utilized in a multidimensional problem. Note that in the latter case we are *not* time splitting the entire transport operator, but only the flux limiter (5). In this way we are testing only the limiters themselves.

In Figure 13 we show a perspective view of the two calculations after $\frac{1}{4}$ revolution (157 iterations). Figure 14 presents a comparison of the results of the two calculations for one full revolution (628 cycles). Two features are obvious. The first is a much greater filling-in of the slot with the time split Eq. (5) than with the fully two dimensional flux limiter. The second is the loss of the bridge connecting the two halves of the cylinder in the case of the time-split application of Eq. (5). Less obvious is the *lack of clipping* of the peaked profiles defining the

front surface of the cylinder for the case of the fully multidimensional limiter. Clearly this is due to the fact that the multidimensional flux limiter can look in *both* directions to determine whether or not a genuine maximum exists. Note that there are *two* factors working in favor of the fully multidimensional flux limiter: 1) the ability to look in *both* directions to find minima and maxima, as just mentioned; and 2) the ability to scan both $w_{i,j}^n$ and $w_{i,j}^{ld}$ to find maxima and minima. Both of these factors are responsible for the improved profiles.

VIII. THE STRIATIONS CODE - A TWO DIMENSIONAL INCOMPRESSIBLE FLUID CODE USING FULLY MULTIDIMENSIONAL FCT

A two dimensional ($\hat{x} - \hat{y}$) plasma cloud initialized in a region of constant magnetic field \mathbf{B}_o directed along the \hat{z} axis, with an externally imposed electric field \mathbf{E}_o directed along the \hat{x} axis will tend to drift in the $\mathbf{E}_o \times \mathbf{B}_o$ direction (along the negative \hat{y} axis) (see Figure 15). If the ion-neutral collision frequency is finite, Pedersen conductivity effects will produce polarization fields which tend to shield the inner (more dense) regions of the cloud from \mathbf{E}_o , causing this inner portion of the cloud to drift more slowly than the outer portions of the cloud. This results in a steepening of gradients on the *back* side of the cloud. Arguments similar to those above, applied to infinitesimal perturbations imposed upon this back side gradient, show that the back side of the cloud is physically unstable to perturbations along \hat{x} . For a detailed description of this problem, see [7].

The equations of motion for the electron fluid are:

$$(\partial N_e / \partial t) + \nabla_{\perp} \cdot (N_e \mathbf{V}_e) = 0 \quad (21)$$

$$\nabla_{\perp} \cdot (N_e \nabla_{\perp} \Psi) = \mathbf{E}_o \cdot \nabla_{\perp} N_e \quad (22)$$

$$\mathbf{V}_e = - (c/B_o) \nabla_{\perp} \Psi \times \hat{z} \quad (23)$$

Here N_e , \mathbf{V}_e , and Ψ are the electron density, electron velocity and perturbation electric field potential respectively, and ∇_{\perp} is the two dimensional divergence operator $\hat{x} \frac{\partial}{\partial x} + \hat{y} \frac{\partial}{\partial y}$.

The magnitudes of \mathbf{B}_o and \mathbf{E}_o are 0.5 gauss and 5 millivolts per meter respectively. Our rest frame here is that of the $(c/B_o)\mathbf{E}_o \times \hat{z}$ velocity. A few trivial vector identities will convince the reader that $\nabla_{\perp} \mathbf{V}_e = 0$, meaning that the electrons move incompressibly. Clearly time-splitting

the transport operator would be disastrous here, and a fully two dimensional scheme is required.

Eq. (22) is solved for Ψ using an elliptic solver, and Eq. (23) then yields the electron velocity field. We then utilize exactly the same multidimensional FCT transport algorithm used in the previous section for solid body rotation to integrate Eq. (21) in time.

Our computational mesh consists of 40 grid points in the \hat{x} direction, 160 grid points in the \hat{y} direction, periodic boundary conditions in both directions, and $\Delta x = \Delta y = 0.31$ km. Our "cloud" consists of a 1-D gaussian:

$$N_e(x,y) = N_o (1 + 10e^{-(y-y_o)^2/64})$$

where N_o is the ambient background electron density and y_o is the spatial center of the gaussian distribution. Superimposed upon this distribution is a random x -dependent perturbation with a maximum amplitude of 3 percent.

Figures 16-20 show isodensity contours of N_e/N_o for the above configuration at various times in the integration. It is seen that, as expected, the back of the cloud (the upper half in the plots) is unstable, growing linearly in the very early stages of development. Non-linear effects soon enter the physics, however, as each striation successively bifurcates, producing smaller and smaller scale structures, in agreement with the results of the ionospheric barium cloud releases which we are attempting to model. Two points which bear on the numerics should be noted: 1) the intense gradients dictated by the physics are *not* diffused away, nor do there appear in the problem any of the "ripples" associated with numerical dispersion which normally appear when steep gradients try to form; 2) precisely because we did not have to resort to time-splitting, none of the usual time splitting phenomena, such as temporal density oscillations and spurious density values, are evident.

CONCLUSIONS

We have shown that the algorithm presented in Eq. (6') through (14'), (17') and (18') does, in fact, represent a workable multidimensional flux limiter. In addition, due to the flexibility in determining overshoot and undershoot criteria inherent in the method, the algorithm

produces results which are consistently equal or superior to those produced using a time-split version of the original flux limiter (5), at least for the admittedly limited class of problems presented here.

For multidimensional problems where time splitting is unacceptable, or for problems where the "clipping" phenomenon associated with the original flux limiter (5) is a serious problem, the new algorithm presented here represents the only way that FCT may be implemented. For these problems the choice is clear, for there is only one option. Yet even in situations where the constraints mentioned above do not apply, benefit may be gained by implementing the new algorithm rather than time splitting Eq. (5). We do not yet have enough experience to give any guidelines, and can only ask the prospective user to try the method.

Certainly the possibilities for modifying the basic scheme are endless. One could, for instance, limit the antidiiffusive fluxes only with respect to maxima, or to minima; or he could limit the fluxes *sequentially* for maxima and minima, rather than limiting maxima and minima simultaneously in the manner presented here (this last procedure will introduce an asymmetry between the treatment of maxima and minima which may or may not be desirable). Even within time-split codes there are possibilities. One could time split the one dimensional form of the new algorithm rather than time splitting Eq. (5); or fully multidimensional flux limiting could be performed at the end of each sweep of a time-split scheme.

On NRL's Texas Instruments ASC computer, the calculations presented in section VII required 93 seconds and 125 seconds of CPU time for the time-split and fully multidimensional cases respectively, a cost penalty of slightly more than 30% for the multidimensional limiter. Of course this extra cost is highly problem dependent. For instance the striations code described in section VIII spends 80% of its time solving Eq. (22), making the net cost penalty of fully multidimensional flux limiting only a few percent.

ACKNOWLEDGEMENTS

I would like to thank Drs. J. Boris, D. Book and J. Gardner for first introducing me to FCT, and for innumerable discussions over the past few years on the subject of transport algorithms. I would also like to especially thank Dr. Book for his indefatigable encouragement. This work was supported by the Defense Nuclear Agency.

REFERENCES

1. J.P. Boris and D.L. Book, Flux-corrected transport. I. SHASTA, a fluid transport algorithm that works, *J. Comp. Phys.* 11 (1973), 38.
2. D.L. Book, J.P. Boris, and K. Hain, Flux-corrected transport. II. Generalizations of the method, *J. Comp. Phys.* 18 (1975), 248.
3. J.P. Boris and D.L. Book, Flux-corrected transport. III. Minimal-Error FCT algorithms, *J. Comp. Phys.* 20 (1976), 397.
4. D. Gottlieb, Strang-type difference schemes for multidimensional problems, *SIAM J. Num. Anal.* 9 (1972), 650.
5. C.K. Forester, Higher order monotonic convective difference schemes, *J. Comp. Phys.* 23 (1977), 1.
6. H.-O. Kreiss and J. Oliger, Comparison of accurate methods for the integration of hyperbolic equations, *Tellus* 24 (1972), 199.
7. A.J. Scannapieco, S.L. Ossakow, S.R. Goldman, and J.M. Pierre, Plasma cloud late time striation spectra, *J. Geophys. Res.* 81(1976), 6037.

Sixth order :

$$F_{i+(1/2)} = \frac{37}{60}(f_{i+1} + f_i) - \frac{2}{15}(f_{i+2} + f_{i-1}) + \frac{1}{60}(f_{i+3} + f_{i-2})$$

Eighth order :

$$F_{i+(1/2)} = \frac{533}{840}(f_{i+1} + f_i) - \frac{139}{840}(f_{i+2} + f_{i-1}) + \frac{29}{840}(f_{i+3} + f_{i-2}) - \frac{1}{280}(f_{i+4} + f_{i-3})$$

The above fourth and eighth order forms are used as the high order fluxes in the main body of this paper.

The low order flux of the leapfrog-trapezoidal FCT schemes is simply donor cell plus a zeroth order diffusive flux with coefficient $\frac{1}{8}$. The donor cell algorithm requires that

$f = vw$, where v is a convective velocity. Specifically,

$$F_{i+(1/2)}^L = v_{i+(1/2)} w_{i+(1/2)}^{DC} - \frac{1}{8}(x_{i+1} - x_i)(w_{i+1}^0 - w_i^0) \Delta t^{-1}$$

where

$$v_{i+(1/2)} \equiv \frac{1}{2}(v_i + v_{i+1})$$

$$w_{i+(1/2)}^{DC} = \begin{cases} w_i^o & \text{if } v_{i+(1/2)} \geq 0 \\ w_{i+1}^o & \text{if } v_{i+(1/2)} < 0 \end{cases}$$

$$w_i^0 = \begin{cases} w_i^{n-1} & \text{for leapfrog step} \\ w_i^n & \text{for trapezoidal step} \end{cases}$$

A detailed description and analysis of these and other high order FCT algorithms will be discussed in a forthcoming report by the present author.

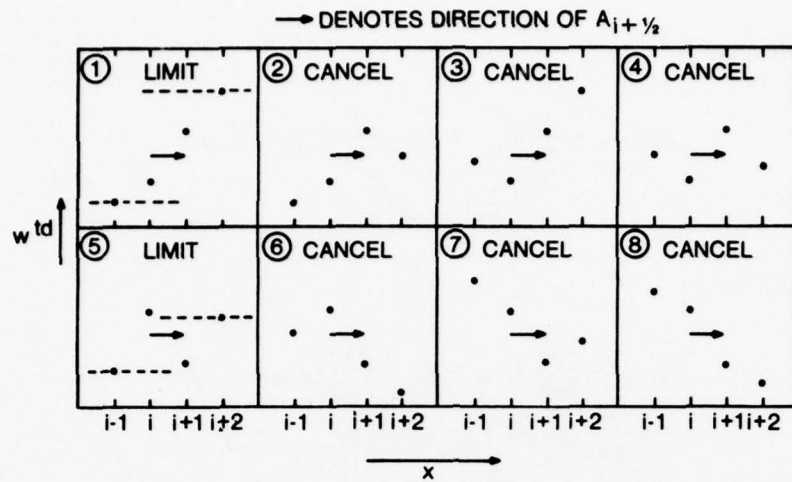


Fig. 1. The eight possible configurations of the transported and diffused solution w^td in the neighborhood of a positive (rightward-directed) antidiffusive flux $A_{i+(1/2)}$. Note that configurations 1 through 4 differ from configurations 5 through 8 only in the sign of the quantity $(w_{i+1}^{td} - w_i^{td})$.

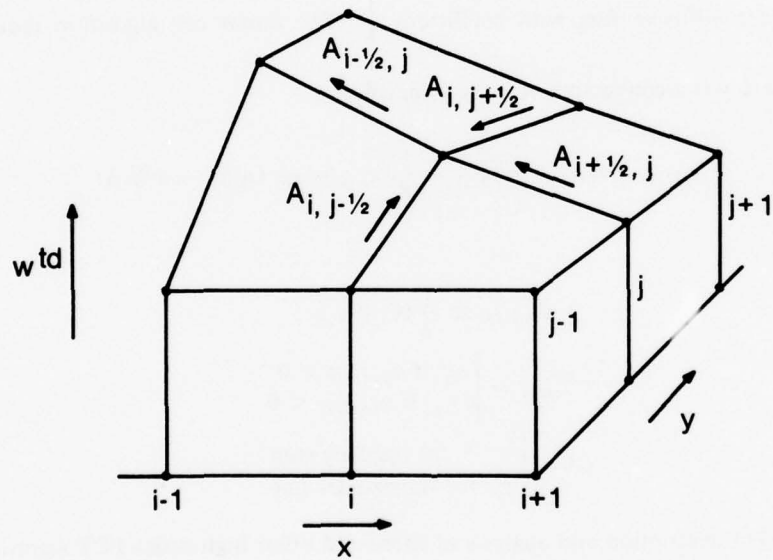


Fig. 2. Perspective view of a two dimensional profile of the transported and diffused solution w^td , showing the four possible antidiiffusive fluxes affecting the grid point (i, j) , the directions of which are indicated by arrows. Note that all of the fluxes are parallel to the local gradient in w^td (as "antidiiffusive" fluxes might be expected to be), and that $w_{i,j}^{td}$ is not an extremum. This situation is impossible in one dimension, and it is precisely this impossibility which allows fluxes to be limited without regard to neighboring fluxes (see text). In two or more spatial dimensions a flux-limiting formula *must* take into account effects due to multiple fluxes acting in concert.

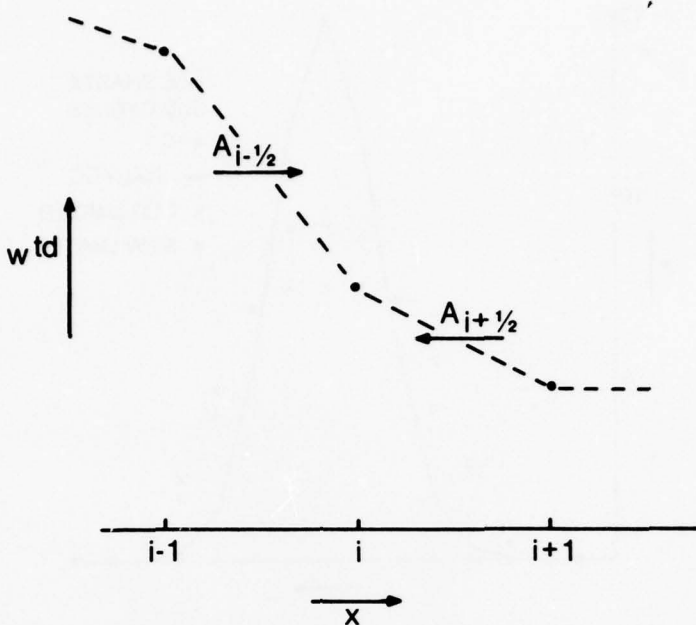


Fig. 3. One dimensional profile of the transported and diffused profile w^{td} , showing the two antidiiffusive fluxes $A_{i+(1/2)}$ and $A_{i-(1/2)}$ whose collective effect must be taken into account with respect to overshoots and undershoots in the final value of w_i^{n+1} .

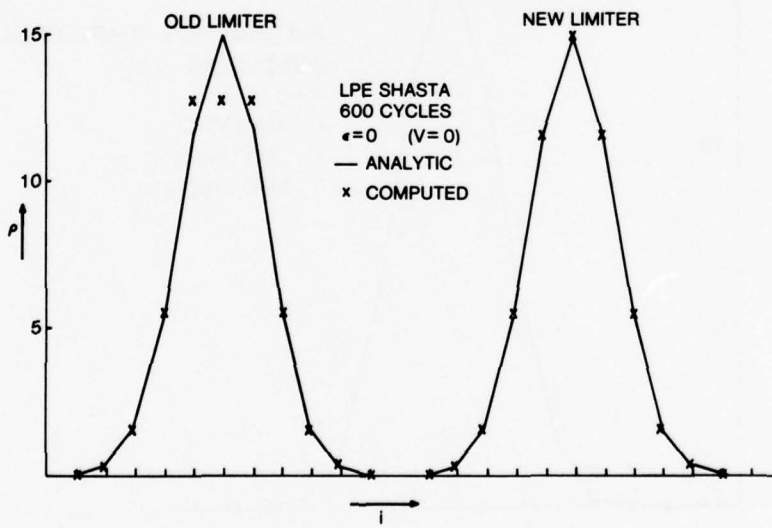


Fig. 4. Comparison of old and new flux limiters on narrow gaussian profile in passive convection for the trivial case of a vanishing velocity field. The transport algorithm is LPE SHASTA. Note the "clipping" phenomenon associated with the old limiter.

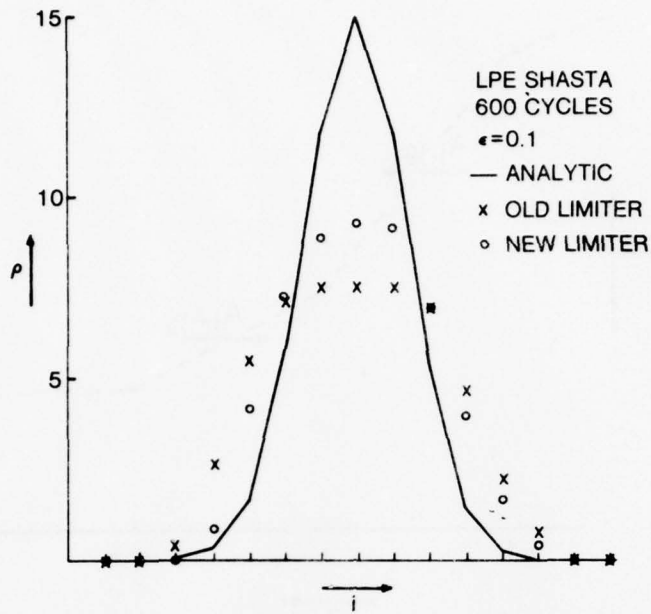


Fig. 5. Same comparison as in Fig. 4 except that the velocity fluid is now finite. The profile has been convected through 60 grid points. Note the reduced clipping with the new flux limiter.

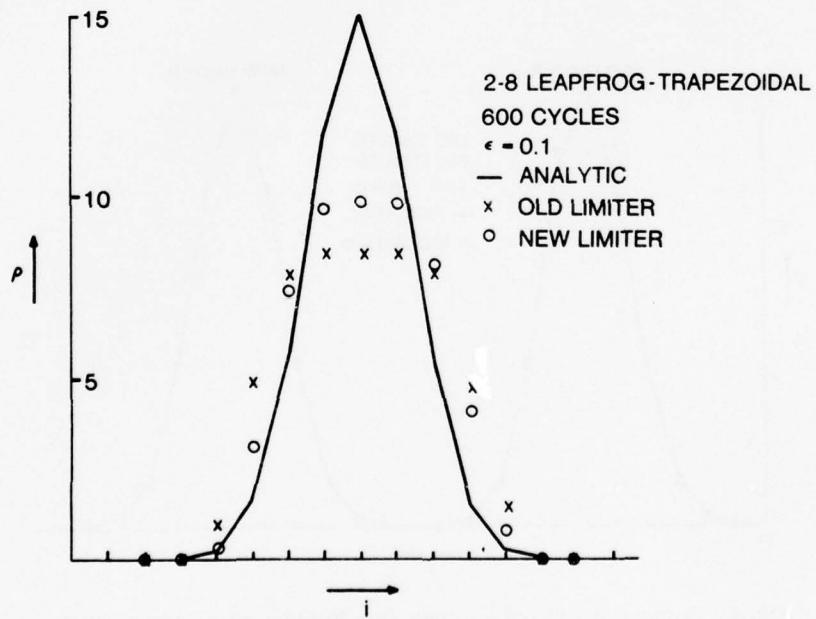


Fig. 6. Same comparison as in Fig. 5, but with a more accurate transport algorithm (2-8 leapfrog-trapezoidal). Again note the reduced clipping with the new flux limiter.

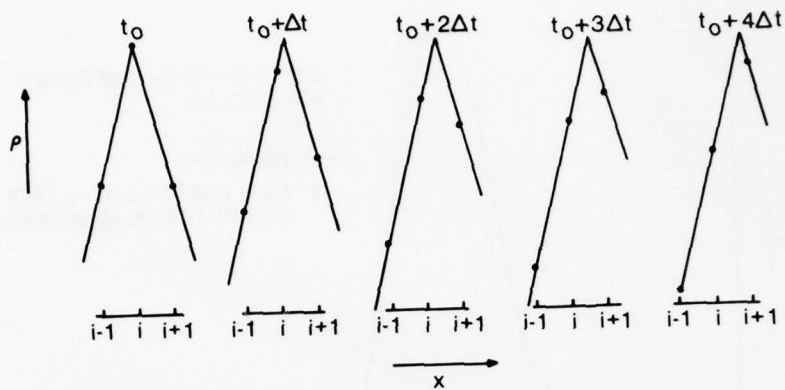


Fig. 7. Time sequence of profiles produced by a "perfect" convection scheme acting on the variable ρ with $\epsilon = 0.2$. The actual analytic profile is shown as a solid line, and the grid point values are shown as dots. Note that at time $t_0 + 4\Delta t$ a grid point value at $(i + 1)$ has been generated which is higher than any grid point value at the previous time step. This is the reason that even the new flux limiter, using Eq. (17) and (18) for w^{\max} and w^{\min} , must still "clip".

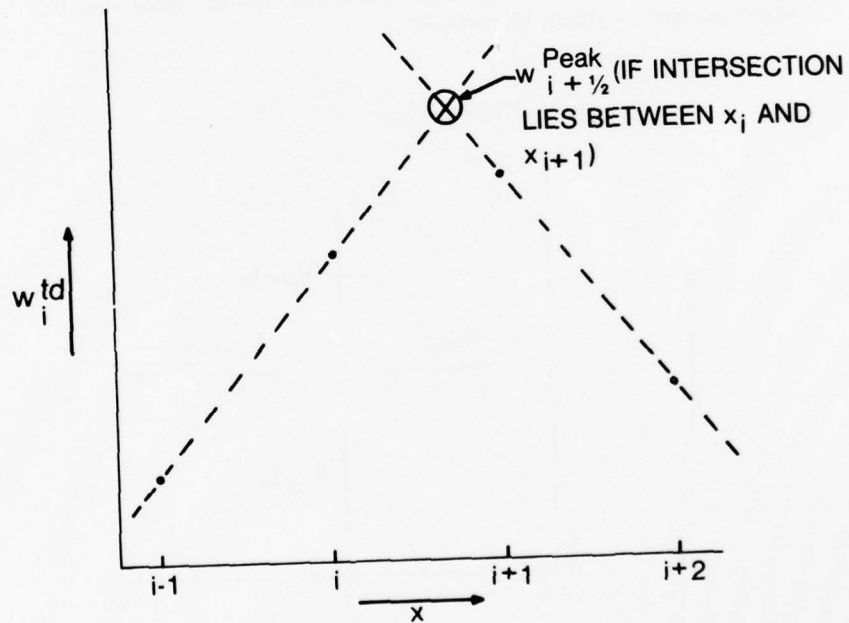


Fig. 8. A possible scheme for extracting information about extrema which exist *between* grid points at a given point in time. An extremum is assumed to exist between grid points i and $i + 1$ if the intersection of the right and left sided extrapolations of w^{\max} has an x coordinate between x_i and x_{i+1} . The w coordinate of the intersection is then used in the computation of w^{\max} and w^{\min} (see text).

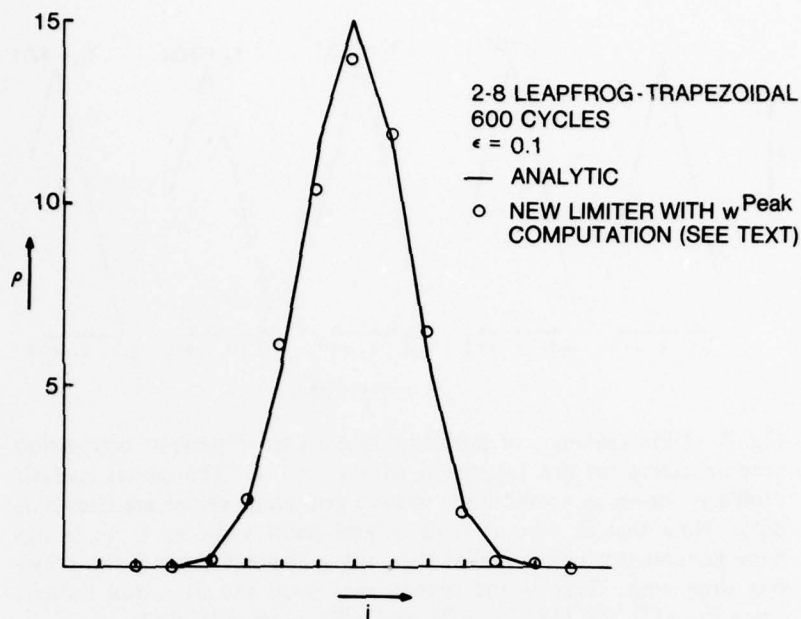


Fig. 9. Same as Fig. 6, except that Eq. (19) and (20), which utilize the w^{peak} computation illustrated in Fig. 8., are used to compute w^{max} and w^{min} in the new flux limiter. Values for the old flux limiter, since they are identical to those shown in Fig. 6, are not shown. Note that the clipping has been virtually eliminated.

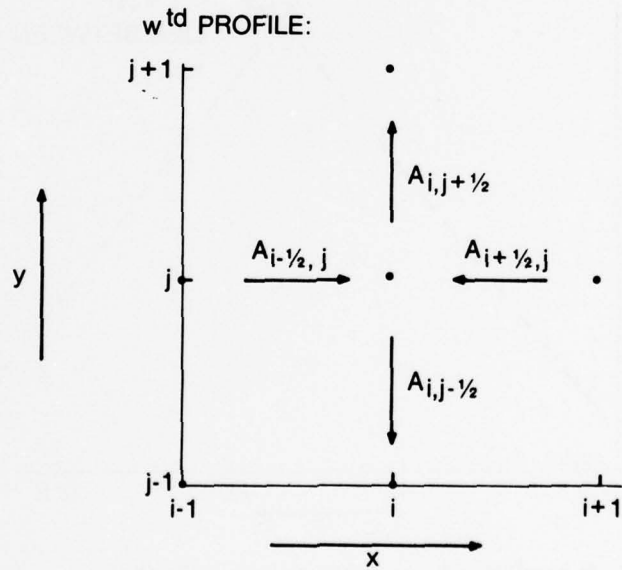


Fig. 10. Two dimensional profile of the transported and diffused values w^{td} , showing the four antidiffusive fluxes $A_{i+1/2, j}$, $A_{i-1/2, j}$, $A_{i, j+1/2}$, and $A_{i, j-1/2}$ whose collective effect must be taken into account with respect to overshoots and undershoots in the final value of $w_{i,j}^{n+1}$. A perspective view of a similar profile is shown in Fig. 2.

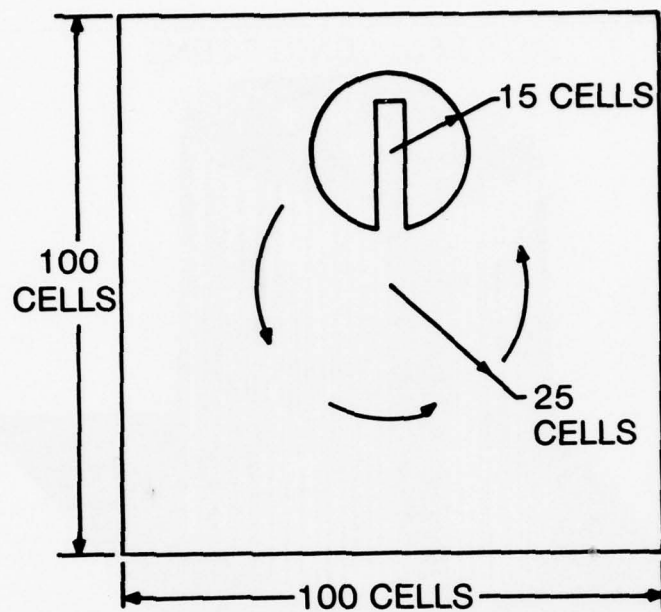


Fig. 11. Schematic representation of two dimensional solid body rotation problem. Initially w inside the cut-out cylinder is 3.0, while outside $w = 1.0$. The rotational speed is such that one full revolution is effected in 628 cycles. The width of the gap separating the two halves of the cylinder, as well as the maximum extent of the "bridge" connecting the two halves, is 5 cells.

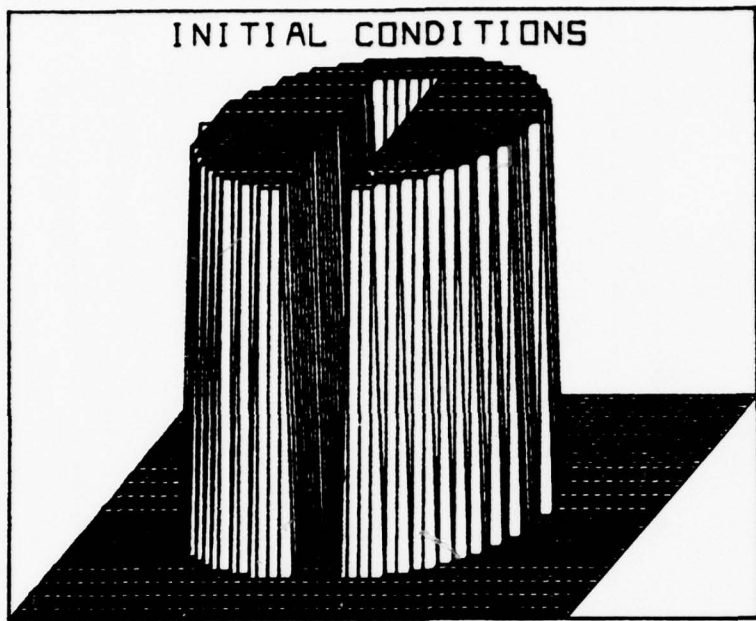


Fig. 12. Perspective view of initial conditions for the two dimensional solid body rotation problem. Note that only a 50×50 portion of the mesh centered on the cylinder is displayed. Grid points inside the cylinder have $w_{i,j} = 3.0$. All others have $w_{i,j} = 1.0$.

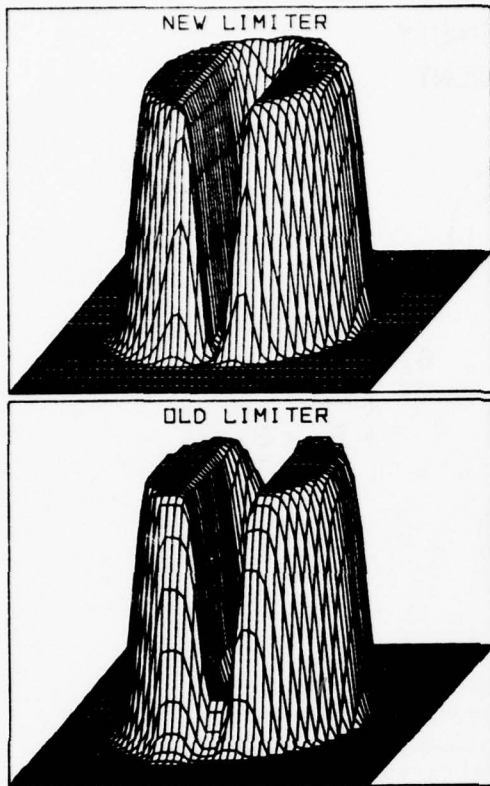


Fig. 13. Comparison of perspective views of the w profile after 157 iterations (1/4 revolution) with both the old and new flux limiters. The perspective view has been rotated with the cylinder, so that direct comparison with Fig. 12 can be made. Again we plot only the 50×50 grid centered on the analytic center of the cylinder. Features to compare are the filling-in of the gap, erosion of the "bridge", and the relative sharpness of the profiles defining the front surface of the cylinder.

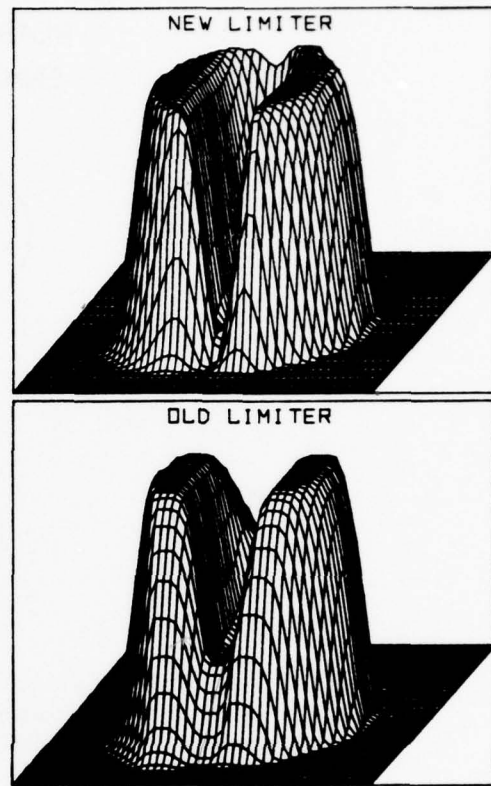


Fig. 14. Same as Fig. 14, but after 628 iterations (one full revolution). Again note decreased diffusion with new flux limiter.

PLASMA DENSITY ENHANCEMENT

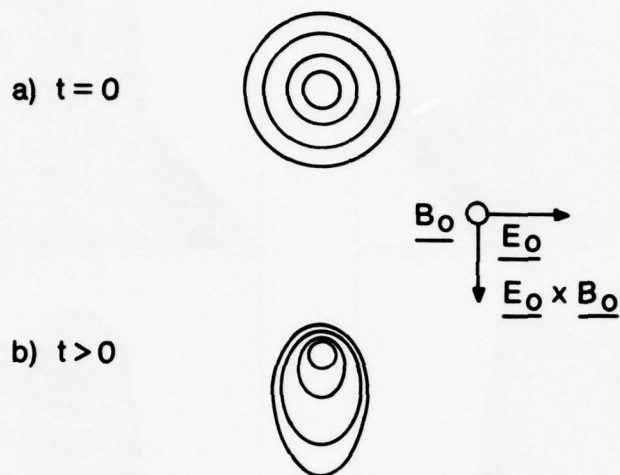
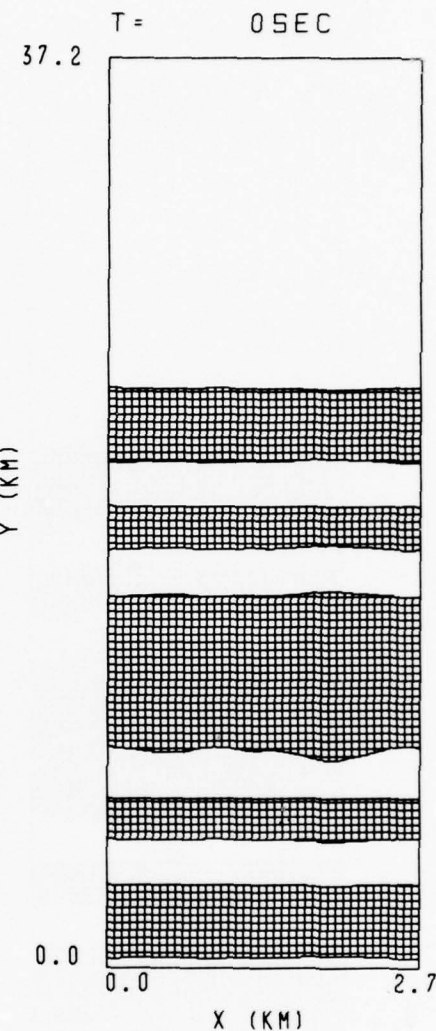


Fig. 15. Schematic representation of the development of a plasma cloud (plasma density increasing toward the center) in crossed electric and magnetic fields. Superimposed on the bulk $E_0 \times B_0$ motion is a steepening of the rearward side of the cloud. This same side is physically unstable to small perturbations.

Fig. 16. Isodensity contours of plasma density at $t = 0$ sec. The initial distribution for N_e/N_o is a gaussian in y , centered at $y = 12.1$ km, plus a small random perturbation in x . Contours are drawn for $N_e/N_o = 1.5, 3.5, 5.5, 7.5$ and 9.5 . The area between every other contour line is cross-hatched. Only 120 of the 160 cells actually used in the y direction are displayed. Boundary conditions are periodic in both directions. In our plot \mathbf{B}_o is toward the reader, and \mathbf{E}_o is directed toward the right, and we have placed ourselves in a frame moving with the $(c/|B_o|^2) \mathbf{E}_o \times \mathbf{B}_o$ velocity. The upper portion of the gaussian is physically unstable to perturbations, while the lower half is (linearly) stable.



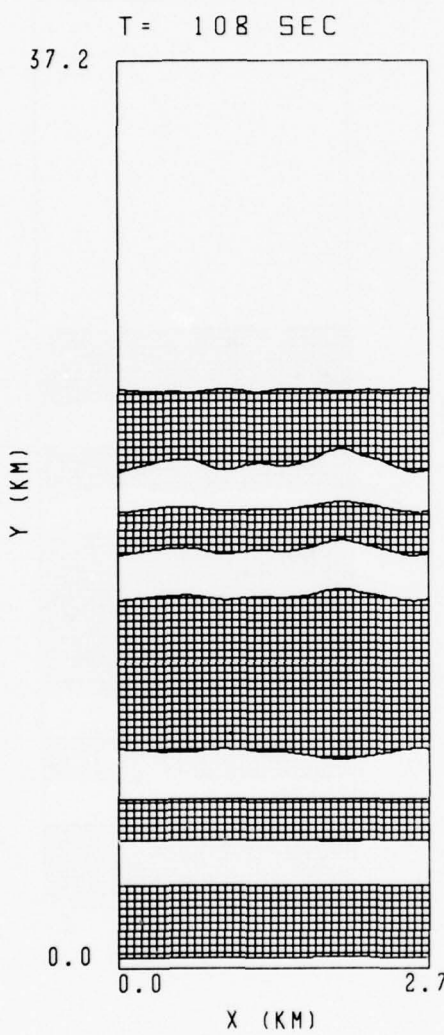


Fig. 17. Same as Fig. 16, but for $t = 108$ sec. Note slow linear growth on unstable side.

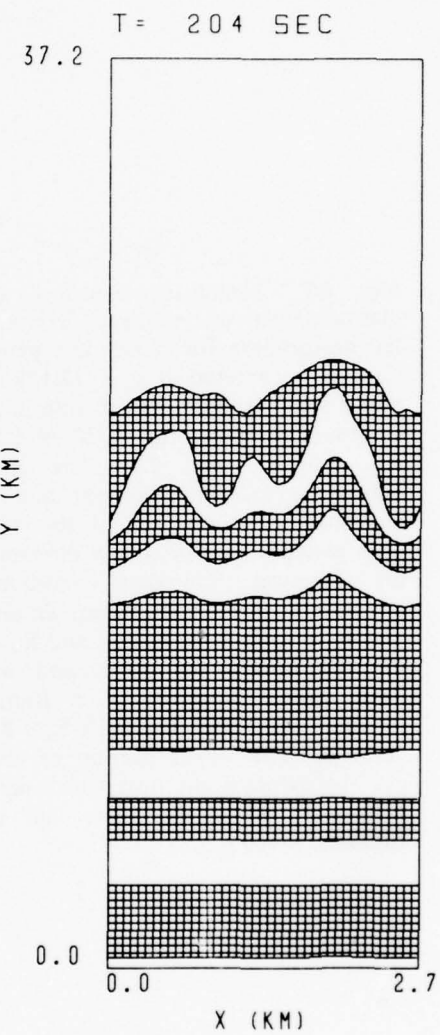


Fig. 18. Same as Fig. 16, but for $t = 204$ sec. Growth is now much more rapid, and we are entering a highly nonlinear regime.

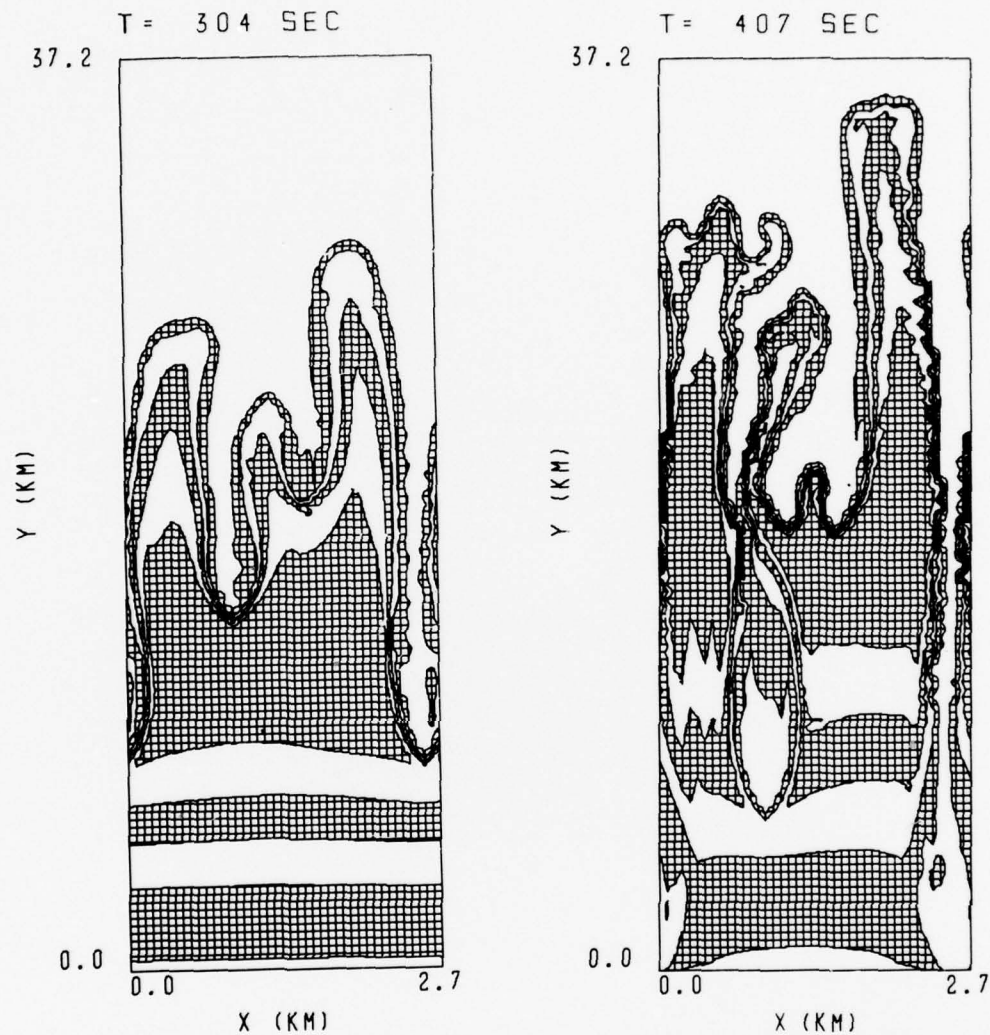


Fig. 19. Same as Fig. 16, but for $t = 304$ sec. Development is fully nonlinear, as the intense gradients and associated high Fourier wave numbers become apparent.

Fig. 20. Same as Fig. 16, but for $t = 407$ sec. Several plasma bifurcations are apparent, in agreement with the experimental results from ionospheric barium cloud releases, and we have maximum to minimum density variations resolved over only 2 cells.

DISTRIBUTION LIST

DIRECTOR
Defense Advanced Rsch Proj Agency
Architect Building
1400 Wilson Blvd.
Arlington, Va. 22209
ATTN: Strategic Tech Office

Defense Communication Engineer Center
1860 Wiehle Avenue
Reston, Va. 22090
ATTN: CODE R820 R. L. Crawford
ATTN: Code R410 W. D. Dehart

DIRECTOR
Defense Communications Agency
Washington, D. C. 20305
ATTN: CODE 960
ATTN: CODE 480

Defense Documentation Center
Cameron Station
Alexandria, Va. 22314
ATTN: TC

12 copies (if open publication)
2 copies (if otherwise)

DIRECTOR
Defense Intelligence Agency
Washington, D. C. 20301
ATTN: W. Wittig DC - 7D
ATTN: DT-1B

DIRECTOR
Defense Nuclear Agency
Washington, D. C. 20305
ATTN: STSI Archives
ATTN: STVL
ATTN: STTL Tech Library
ATTN: DDST
ATTN: RAAE

2 copies

DIR OF DEFENSE RSCH & ENGINEERING
Washington, D. C. 20301
ATTN: DD/S&SS John B. Walsh
ATTN: OAD/EPS

COMMANDER
Field Command
Defense Nuclear Agency
Kirtland AFB, NM 87115
ATTN: FCPR
ATTN FCPR COL. John P. Hill
Interservice Nuclear Weapons School
Kirtland AFB, NM 87115
ATTN: Document Control

DIRECTOR
Joint Strat TGT Planning Staff Jcs
Offutt AFB
Omaha, NB 68113
ATTN: JLTW-2
ATTN: JPST G. D. Burton
ATTN: JPST MAJ. J. S. Green

CHIEF
Livermore Division Fld Command DNA
Lawrence Livermore Laboratory
P. O. Box 808
Livermore, CA 94550
ATTN: FCPRL

COMMANDER
National Military Comd Sys Support Ctr
Pentagon
Washington, D. C. 20301
ATTN: B211
ATTN: DP DIRECTOR FOR CSPO

DIRECTOR
National Security Agency
Ft. George G. Meade, Md. 20755
ATTN: W14 Pat Clark
ATTN: Frank Leonard

OJCS/J-3
The Pentagon
Washington, D. C. 20301
ATTN: J-3 OPS ANAL BR. COL. Longberry

OJCS/J-6
The Pentagon
Washington, D. C. 20301
ATTN: J-6

DIRECTOR
Telecommunications & Comd & Con Sys
Washington, D. C. 20301
ATTN: ASST DIR Info & Space Sys
ATTN: DEP ASST. SEC Sys

Weapons Systems Evaluation Group
400 Army-Navy Drive
Arlington, Va. 22202
ATTN: DOCUMENT CONTROL

COMMANDER
Harry Diamond Laboratories
2800 Powder Mill Road
Adelphi, Md. 20783
ATTN: AMXDO-NP

COMMANDER
TRASANA
White Sands Missile Range, NM 88002
ATTN: EAB

DIRECTOR
U. S. Army Ballistic Research Labs
Aberdeen Proving Ground, Md. 21003
ATTN: AM-CA Franklin E. Niles

U. S. Army Communications CMD
C-B Services Division
Pentagon Rm. 2D513
Washington, D. C. 20310
ATTN: CEAD

COMMANDER
U. S. Army Electronics Command
Fort Monmouth, N. J. 07703
ATTN: AMSEL-TL-ENV Hans A. Bomke

COMMANDER
U. S. Army Material Command
5001 Eisenhower Avenue
Alexandria, Va. 22332
ATTN: AMCRD-WN-RE John F. Corrigan

COMMANDER

U. S. Army Material Command
Foreign and Scientific Tech Center
220 7th St. N. E.
Charlottesville, Va. 22901
ATTN: P. A. Crowley
ATTN: R. Jones

COMMANDER

U. S. Army Missile Command
Redstone Arsenal
Huntsville, Al. 35809
ATTN: AMSMI-YTT W. G. Preussel, Jr.

COMMANDER

U. S. Army Nuclear Agency
Fort Bliss, Tx. 79916
ATTN: USANUA-W. J. Berbert
ATTN: CDINS-E

CHIEF of Naval Research

Department of the Navy
Arlington, Ba. 22217
ATTN: CODE 464 Jacob L. Warner
ATTN: CODE 464 Thomas P. Quinn

COMMANDER

Naval Air Systems Command
Headquarters
Washington, D. C. 21360
ATTN: AIR 5381

COMMANDER

Naval Electronics Systems Command
Naval Electronic System CMD HQS
Washington, D. C. 20360
ATTN: NAVALEX 034 T. Barry Hughes
ATTN: PME 106-1 Satellite Comm Project Off
ATTN: John E. Doncarlos
ATTN: PME 117

COMMANDER

Naval Electronics Laboratory Center
San Diego, CA 92152
ATTN: William F. Moler
ATTN: CODE 2200 Verne E. Hildebrand
ATTN: R. Eastman

COMMANDING OFFICER
Naval Intelligence Support CTR
1301 Suitland Road, Bldg. 5
Washington, D. C. 20390
ATTN: Mr. Dubbin Stic 12

DIRECTOR
Naval Research Laboratory
Washington, D. C. 20375
ATTN: HQ COMM DIR Bruce Wald
ATTN: CODE 5460 Radio Propagation BR
ATTN: CODE 6701 Jack D. Brown
ATTN: CODE 6700 Division Superintendent
ATTN: CODE 6750 Branch Head
ATTN: CODE 7127, Chas. Y. Johnson

25 copies (if unclass)
1 copy (if classified)
150 copies (if unclass)
1 copy (if classified)

COMMANDING OFFICER
Naval Space Surveillance System
Dahlgren, Va. 22448
ATTN: CAPT. J. H. Burton

COMMANDER
Naval Surface Weapons Center
White Oak, Silver Spring, Md. 20910
ATTN: CODE 1224 Navy Nuc Prgms Off
ATTN: CODE 730 Tech. Lib.

DIRECTOR
Strategic Systems Project Office
Navy Department
Washington, D. C. 20376
ATTN: NSP-2141

COMMANDER
ADC/AD
ENT AFB, Co., 80912
ATTN: ADDA

Headquarters
U. S. Army Elect Warfare Lab (ECOM)
White Sands Missile Range, NM 88002
ATTN: E. Butterfield

AF Cambridge Rsch Labs, AFSC
L. G. Hanscom Field
Bedford, Ma 01730
ATTN: LKB Kenneth S. W. Champion
ATTN: OPR James C. Ulwick
ATTN: OPR Hervey P. Gauvin

AF Weapons Laboratory, AFSC
Kirtland AFB, NM 87117

ATTN: John M. Kamm SAS
ATTN: SUL
ATTN: DYT LT Mark A. Fry
ATTN: DYT CAPT Wittwer
ATTN: DYT CAPT Gary Cable

AFTAC

Patrick AFB, Fl. 32925

ATTN: TF MAJ. E. Hines
ATTN: TF/CAPT. Wiley
ATTN: TN

Air Force Avionics Laboratory, AFSC
Wright-Patterson AFB, Oh. 45433
ATTN: AFAL AWWE Wade T. Hunt

Assistant Chief of Staff
Studies and Analysis
Headquarters, U. S. Air Force
Washington, D. C. 20330

Headquarters
Electronics Systems Division (AFSC)
L. G. Hanscom Field
Bedford, Ma. 01730
ATTN: XRE LT. Michaels
ATTN: LTC J. Morin CDEF XRC
ATTN: YSEV

COMMANDER
Foreign Technology Division, AFSC
Wright-Patterson AFB, Oh. 45433
ATTN: TD-BTA LIBRARY

HQ USAF/RD
Washington, D. C. 20330
ATTN: RDQ

COMMANDER
Rome Air Development Center, AFSC
Griffith AFB, N. Y. 13440
ATTN: EMTLD Doc Library

COMMANDER IN CHIEF
Strategic Air Command
Offutt AFB, NB 68113
ATTN: XPFS MAJ. Brian G. Stephan

544IES

Offutt AFB, NB 68113

ATTN: RDPO LT. Alan B. Merrill

Los Alamos Scientific Laboratory

P. O. Box 1663

Los Alamos, NM 87544

ATTN: DOC CON for R. F. Taschek

ATTN: DOC CON for Milton Peek

ATTN: DOC CON for Eric Lindman

Sandia Laboratories

P. O. Box 5800

Albuquerque, NM 87115

ATTN: DOC CON for A. Dean Thronbrough

ATTN: DOC CON for W. D. Brown

ATTN: DOC CON for D. A. Dahlgren, ORG 1722

ATTN: DOC CON for J. P. Martin, ORG 1732

University of California

Lawrence Livermore Laboratory

P. O. Box 808

Livermore, CA 94550

ATTN: Tech Info Dept L-3

Department of Commerce

National Oceanic & Atmospheric Admin.

Environmental Research Laboratories

Boulder, CO 80302

ATTN: Joseph H. Pope

ATTN: C. L. Rufenach

Department of Commerce

Office for Telecommunications

Institute for Telecom Science

Boulder, CO 80302

ATTN: Glenn Falcon

ATTN: G. Reed

ATTN: L. A. Berry

ATTN: William F. Utlaut

Department of Transportation

Transportation Rsch. System Center

Kendall Square

Cambridge, MA 02142

ATTN: TER G. Harowles

NASA

Goddard Space Flight Center

Greenbelt, Md 20771

ATTN: CODE 750 T. Golden

NASA
600 Independence Ave., S. W.
Washington, D. C. 20346
ATTN: M. Dubin

Aerodyne Research, Inc.
Tech/Ops Building
20 South Avenue
Burlington, MA 01803
ATTN: M. Camac
ATTN: F. Bien

Aerospace Corporation
P. O. Box 92957
Los Angeles, CA 90009
ATTN: T. M. Salmi
ATTN: S. P. Bower
ATTN: V. Josephson
ATTN: SMFA for FWW
ATTN: R. Grove
ATTN: R. D. Rawcliffe
ATTN: T. Taylor
ATTN: Harris Mayer
ATTN: D. C. Cartwright

Analytical Systems Corporation
25 Ray Avenue
Burlington, MA 01803
ATTN: Radio Sciences

Avco-Everett Research Laboratory, Inc.
2385 Revere Beach Parkway
Everett, MA 02149
ATTN: Richard M. Patrick

Boeing Company, The
P. O. Box 3707
Seattle, WA 98124
ATTN: D. Murray
ATTN: Glen Keister

Brown Engineering Company, Inc.
Cummings Research Park
Huntsville, AL 35807
ATTN: David Lambert MS 18

California at San Diego, Univ. of
Building 500 Mather Campus
3172 Miramar Road
La Jolla, CA 92037
ATTN: Henry G. Booker

Calspan
P. O. Box 235
Buffalo, N. Y. 14221
ATTN: Romeo A. Deliberis

Computer Sciences Corporation
P. O. Box 530
6565 Arlington Blvd.
Falls Church, VA 22046
ATTN: H. Blank
ATTN: Barbara F. Adams

Comsat Laboratories
P. O. Box 115
Clarksburg, Md. 20734
ATTN: R. R. Taur

Cornell University
Department of Electrical Engineering
Ithaca, N. Y. 14850
ATTN: D. T. Farley, Jr.

ESL, Inc.
495 Java Drive
Sunnyvale, CA 93102
ATTN: J. Roberts
ATTN: V. L. Mower
ATTN: James Marshall
ATTN: R. K. Stevens

General Electric Company
Tempo-Center for Advanced Studies
816 State Street
Santa Barbara, CA 93102
ATTN: Don Chandler
ATTN: DASIAC
ATTN: Tim Stephens

General Electric Company
P. O. Box 1122
Syracuse, N. Y. 13201
ATTN: F. A. Reibert

General Research Corporation
P. O. Box 3587
Santa Barbara, CA 93105
ATTN: John Ise, Jr.

Geophysical Institute
University of Alaska
Fairbanks, AK 99701
ATTN: Technical Library
ATTN: Neil Brown
ATTN: T. N. Davis

GTE Sylvania, Inc.
189 B Street
Needham Heights, MA 02194
ATTN: Marshall Cross

HRB-SINGER, Inc.
Science Park, Science Park Road
P. O. Box 60
State College, PA 16801
ATTN: Larry Feathers

Honeywell Incorporated
Radiation Center
2 Forbes Road
Lexington, MA 02173
ATTN: W. Williamson

Illinois, University of
Department of Electrical Engineering
Urbana, IL 61801
ATTN: K. C. Yeh

Institute for Defense Analyses
400 Army-Navy Drive
Arlington, VA 22202
ATTN: Ernest Bauer
ATTN: Hans Wolfhard
ATTN: J. M. Aein
ATTN: Joel Bengston

Intl Tel & Telegraph Corporation
500 Washington Avenue
Nutley, N. J. 07110
ATTN: Technical Library

ITT Electro-Physics Laboratories, Inc.
9140 Old Annapolis Road
Columbus, Md. 21043
ATTN: John M. Kelso

Johns Hopkins University
Applied Physics Laboratory
8621 Georgia Avenue
Silver Spring, MD 20910
ATTN: Document Librarian

Lockheed Missiles & Space Co., Inc.
P. O. Box 504
Sunnyvale, CA 94088
ATTN: Dept. 60-12

Lockheed Missiles and Space Company
3251 Hanover Street
Palo Alto, CA 94304
ATTN: Billy M. McCormac, Dept 52-14
ATTN: Martin Walt, Dept 52-10
ATTN: Richard G. Johnson, Dept 52-12
ATTN: JOHN CLADIS

MIT Lincoln Laboratory
P. O. Box 73
Lexington, MA 02173
ATTN: Mr. Walden, X113
ATTN: D. Clark
ATTN: James H. Pannell, L-246
ATTN: Lib A-082 for David M. Towle

Martin Marietta Corporation
Denver Distribution
P. O. Box 179
Denver, CO 80201
ATTN: Special Projects Program 248

Maxwell Laboratories, Inc.
9244 Balboa Avenue
San Diego, CA 92123
ATTN: A. J. Shannon
ATTN: V. Fargo
ATTN: A. N. Rostocker

McDonnell Douglas Corporation
5301 Bolsa Avenue
Huntington Beach, CA 92657
ATTN: J. Moule
ATTN: N. Harris

Mission Research Corporation

735 State Street

Santa Barbara, CA 93101

ATTN: R. Hendrick

ATTN: Conrad L. Longmire

ATTN: Ralph Kilb

ATTN: R. E. Rosenthal

ATTN: R. Bogusch

ATTN: David Sowle

ATTN: M. Scheibe

ATTN: P. Fischer

Mitre Corporation, The

Route 62 and Middlesex Turnpike

P. O. Box 208

Bedford, MA 01730

ATTN: Chief Scientist W. Sen

ATTN: S. A. Morin M/S

ATTN: C. Harding

North Carolina State Univ At Raleigh

Raleigh, N. C. 27507

ATTN: SEC Officer for Walter A. Flood

Pacific-Sierra Research Corp.

1456 Cloverfield Blvd.

Santa Monica, CA 90404

ATTN: E. C. Field, Jr.

Philco-Ford Corporation

Western Development Laboratories Div

3939 Fabian Way

Palo Alto, CA 94303

ATTN: J. T. Mattingley MS X22

Photometrics, Inc.

442 Marrett Road

Lexington, MA 02173

ATTN: Irving J. Kofsky

Mitre Corporation, The

Westgate Research Park

1820 Dolley Madison Blvd.

McLean, VA 22101

ATTN: Allen Schneider

Physical Dynamics, Inc.
P. O. Box 1069
Berkeley, CA 94701
ATTN: Joseph B. Workman

Physical Sciences, Inc.
607 North Avenue, Door 18
Wakefield, MA 01880
ATTN: Kurt Wray

R & D Associates
P. O. Box 3580
Santa Monica, CA 90403
ATTN: Robert E. Lelevier
ATTN: Forest Gilmore
ATTN: Richard Latter
ATTN: William B. Wright, Jr.

R & D Associates
1815 N. Ft. Myer Drive
11th Floor
Arlington, VA 2209
ATTN: Herbert J. Mitchell

Rand Corporation, The
1700 Main Street
Santa Monica, CA 90406
ATTN: Cullen Crain

Science Applications, Inc.
P. O. Box 2351
La Jolla, CA 92038
ATTN: Daniel A. Hamlin
ATTN: D. Sachs
ATTN: E. A. Straker

Space Data Corporation
1331 South 26th Street
Phoenix, AZ 85034
ATTN: Edward F. Allen

Stanford Research Institute
333 Ravenswood Avenue
Menlo Park, CA 94025
ATTN: M. Baron
ATTN: L. L. Cobb
ATTN: Walter G. Chestnut
ATTN: David A. Johnson
ATTN: Charles L. Rino
ATTN: E. J. Fremouw
ATTN: Ray L. Leadabrand
ATTN: Donald Neilson

Stanford Research Institute
306 Wynn Drive, N. W.
Huntsville, AL 35805
ATTN: Dale H. Davis

Technology International Corporation
75 Wiggins Avenue
Bedford, MA 01730
ATTN: W. P. Boquist

TRW Systems Group
One Space Park
Redondo Beach, CA 90278
ATTN: P. H. Katsos
ATTN: J. W. Lowery

Utah State University
Logan, UT 84321
ATTN: C. Wyatt
ATTN: D. Burt
ATTN: Kay Baker
ATTN: Doran Baker

Visidyne, Inc.
19 Third Avenue
North West Industrial Park
Burlington, MA 01803
ATTN: William Reidy
ATTN: Oscar Manley
ATTN: J. W. Carpenter

ED
78